Characterization of FSBS Radial Acoustic Modes in Short Optical Fibers With an All-Fiber Ring Resonator

Anna I. Garrigues-Navarro, Martina Delgado-Pinar, Antonio Díez, and Miguel V. Andrés, *Life Senior Member, IEEE*

***Abstract*—A highly efficient approach for the interrogation of mechanical vibrations excited by forward-stimulated Brillouin scattering in optical fibers is reported. The method is based on an all-fiber ring resonator. The section of optical fiber in which the FSBS takes place is inserted into the loop. Mechanical oscillations modulate the phase of the light propagating through the fiber loop, resulting in the modulation of the ring transmittance. The method takes advantage of the resonant character of the ring transfer function. It has a very high sensitivity and allows the interrogation of mechanical oscillations excited by FSBS in very short fiber sections. Sub-centimeter recognition is demonstrated in this work. Differences between co- and contra-propagating pump and probe signals are investigated.**

***Index Terms*—Forward-stimulated Brillouin scattering (FSBS), optical fiber sensing, optical fibers, opto-mechanics, resonator.**

I. Introduction

RECENT developments based on forward stimulated Brillouin scattering (FSBS) in optical fibers have arisen the interest on this opto-mechanical interaction. Although several works have been reported proposing applications in different fields [1], [2], [3], [4], fiber optic sensing seems to be the area in which FSBS can contribute greatly to improve the state of the art and broaden the range of applications [5], [6], [7], [8], [9], [10], [11], [12], [13].

FSBS is a particular type of Brillouin interaction that involves two optical waves and an acoustic wave that co-propagate in the optical waveguide. Electrostriction is the physical mechanism that drives the optical stimulation of the acoustic wave. In single-mode optical fibers, phase-matching is fulfilled for guided acoustic modes close to their cutoff frequency. Owing to the symmetry of the optical and acoustic fields, only two type of acoustic modes can be stimulated by FSBS, i.e., pure radial acoustic modes, $R_{0,m}$, and torsional-radial modes with angular order 2, $TR_{2,m}$ Many FSBS-based applications in fiber optics rely on $R_{0,m}$ modes as they exhibit a stronger, polarization-independent interaction with the fiber mode. The cutoff frequency of the different acoustic modes depends on the fiber radius and the shear and/or longitudinal acoustic velocities in the fiber [2], [14]. The frequency range in which acoustic modes are excited by FSBS in conventional optical fibers can exceed 1 GHz.

The detection of acoustic modes stimulated by FSBS is commonly performed by optical means. Torsional-radial modes introduce optical birefringence in the fiber, thus, they can be detected though polarization analysis of a probe optical wave. Recently, we reported probing of $TR_{2,m}$ acoustic modes in fiber section with length in the mm scale [15]. In the case of radial modes, acoustic oscillation leads to phase modulation of a probe optical beam propagating in the fiber. Commonly, experimental characterization of $R_{0,m}$ modes is performed by optical interferometry. The Sagnac interferometer is preferred because of its intrinsic insensitivity to changes of environmental conditions. As the magnitude of the FSBS nonlinear coefficient in conventional optical fibers is small, on the order of few $W^{-1}km^{-1}$ [16], interferometric methods require large interaction lengths to provide sufficient sensitivity, usually tens or even hundreds of meters of optical fiber. The requirement of such a fiber length can be a drawback, at least in relation to the development of fiber sensing applications. On the one hand, it limits the development of opto-mechanical, truly point fiber optic sensors using FSBS. Some applications may require the use of short (point) sensors, for instance, in biosensing where sample volume may be limited [17]. In addition, it can have a negative impact on sensor performance, in particular by degrading the detection limit. Most sensor applications are based on the sensitivity of the cut-off frequency of the acoustic modes with the magnitude to be measured [6], [7], [8], [9], [10], [11]. The requirement for such a long fiber length forces in many cases the use of coated optical fibers, which results in a very significant spectral broadening of the stimulated acoustic oscillation due to the high acoustic damping that the polymer coating introduces. Such a contribution to spectral broadening can in part be reduced by using polyimide coated fibers [18], [19], [20] instead of the

Received 7 February 2025; revised 11 April 2025; accepted 4 May 2025. Date of publication 7 May 2025; date of current version 4 August 2025. This work was supported by Horizon 2020 Framework Programme under Grant H2020-MSCA-RISE-2019-872049, in part by Generalitat Valenciana under Grant CIPROM/2022/30 and Grant CIACIF/2023/418, and in part by Ministerio de Ciencia, Innovación y Universidades under Grant CNS2023-145717 and Grant PID2023-146725OB-I00. *(Corresponding author: Antonio Díez.)*

The authors are with Departamento de Física Aplicada y Electromagnetsimo - ICMUV, Universidad de Valencia (Spain), 46010 Valencia, Spain (e-mail: antonio.diez@uv.es).

Color versions of one or more figures in this article are available at https://doi.org/10.1109/JLT.2025.3567858.

Digital Object Identifier 10.1109/JLT.2025.3567858

standard dual-layer acrylate coating. However, even in the case of bare optical fibers, the linewidth of the stimulated acoustic oscillation also increases with fiber length due to an increased presence of inhomogeneities along the fiber, ultimately leading to a worsening of the detection limit.

In recent years, several methods to probe FSBS-stimulated radial acoustic modes that can work with short fiber sections have been reported [21]. Some methods rely on the interplay between the acoustic mode and an optical resonance. The oscillation of the acoustic mode in the optical fiber causes the shift of the optical resonance. Therefore, by monitoring the optical resonance, information about the acoustic mode can be retrieved. With optical resonances produced by long-period gratings [22] and Bragg gratings [9], [23], it was demonstrated that few centimeters of optical fiber were sufficient to detect acoustic modes stimulated by optical pulses with peak power in the range of tens of wats. Recently, the narrowest acoustic mode linewidths ever reported were obtained by probing with high Q factor optical whispering-gallery mode (WGM) resonances of the optical fiber, a technique that requires less than 1 mm of optical fiber [24].

Following this concept, in this paper we report a novel method to probe acoustic modes excited by FSBS in optical fibers using an all-fiber ring resonator. The resonant response of the ring provides sufficient sensitivity for probing FSBS acoustic modes with short fiber segments and moderate pump powers. It is a simple and versatile method, the performance requirements of the ring are quite flexible, and it is not necessary to process the optical fiber or use thin tapered fibers.

II. Theoretical Concepts

A short optical pump pulse propagating in a single-mode optical fiber stimulates an acoustic wave packet made of the superposition of multiple radial and torsional-radial modes [1]. The amplitude with which each acoustic mode is excited depends on the pump pulse characteristics, i.e., peak power and temporal profile, and the mode field diameter of the fiber at the pump wavelength. A detailed theoretical study of the excitation amplitude of the different acoustic modes by the propagation of a pump pulse in a single-mode optical fiber can be found in [16].

Owing to the photo-elastic effect, the oscillation of an acoustic mode causes a refractive index modulation in the optical fiber that can be expressed as,

$$\Delta n\ (r, \phi, z, t) = \Delta n_0\ (r, \phi) \cdot \cos(\Omega \cdot t - q \cdot z) \tag{1}$$

where Ω and q are the frequency and wavenumber of the acoustic mode, respectively, and Δn_0 is an amplitude that depends on the strength and field distribution of the acoustic mode. When such an acoustic mode is excited by FSBS, the fulfilment of the phase-matching condition for the optical stimulation establishes that $q = \Omega/v_p$, where v_p is the phase velocity of the optical pump.

The modulation of the refractive index, in turn, modulates the effective index of an optical probe wave propagating along the optical fiber. Such a perturbation depends on whether the acoustic wave and the optical probe wave are co-propagating

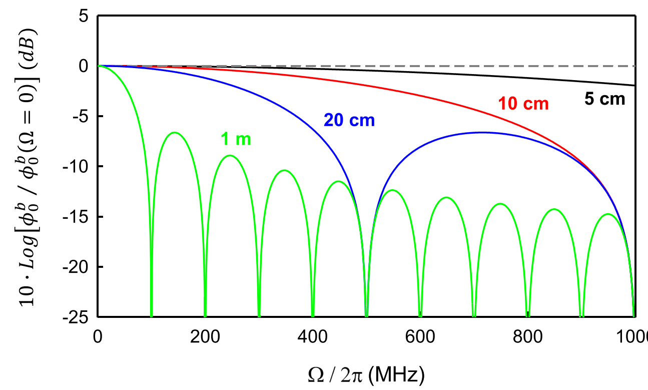

Fig. 1. Normalized ϕ_0^b as a function of frequency, for different fiber length. $v_p = 2.07 \times 10^8$ m/s has been considered for calculations.

or counter-propagating. In the first case, phase-matching is automatically satisfied thus,

$$\Delta n_{eff}\ (z, t) = \xi \cdot \cos(\Omega \cdot t) \tag{2}$$

where ξ is an amplitude that depends on the strength of the acoustic mode, its attenuation factor, and the overlapping between the acoustic and optical fields [16]. When the acoustic mode and the probe counter-propagate, the effective index perturbation can be expressed as,

$$\Delta n_{eff}\ (z, t) = \xi \cdot \cos\left(\Omega \cdot \left(t - \frac{2z}{v_p} + \frac{L_{FUT}}{v_p}\right)\right) \tag{3}$$

where L_{FUT} is the interaction length between the acoustic wave and the optical probe signal. For simplicity, equal phase velocity for optical pump and probe waves is assumed in (2) and (3).

A probe light beam propagating along the interaction region, accumulates a time-varying phase delay $\phi_{AC}(t)$, that can be calculated by,

$$\phi_{AC}\ (t) = k_0 \int_0^{L_{FUT}} \Delta n_{eff}\,(z, t) \cdot dz \tag{4}$$

where k_0 is the optical wavenumber of the probe light. For both, co- and counter-propagation, $\phi_{AC}(t)$ can be expressed as,

$$\phi_{AC}\ (t) \equiv \phi_0^i \cdot \cos(\Omega \cdot t) \tag{5}$$

where $\phi_0^i (i = a, b)$ is the amplitude in the co-propagation and counter-propagation configurations, respectively, that takes the form,

$$\phi_0^a = k_0 \cdot L_{FUT} \cdot \xi \tag{6}$$

and,

$$\phi_0^b = (k_0 \cdot L_{FUT} \cdot \xi)\ \cdot sinc\left(\frac{\Omega \cdot L_{FUT}}{v_p}\right) \tag{7}$$

The effect of the sinc function factor on ϕ_0^b in (7) depends on $(\Omega \cdot L_{FUT}/v_p)$. Fig. 1 shows ϕ_0^b as a function of frequency for different L_{FUT} values. For a fiber length of 10 cm, the first zero crossing of the sinc function occurs at ~1 GHz. Thus, in the frequency range of interest, ϕ_0^b decreases smoothly with frequency, while in the co-propagating case does not change with frequency (see (6)). As the fiber length is increased, the first

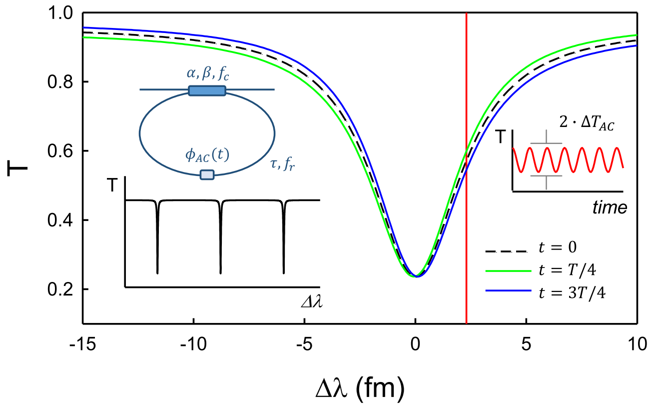

Fig. 2. Transmission of an all-fiber ring vs. optical wavelength around a notch, at different instants of time (indicated) when an acoustic wave of frequency $\Omega = 2\pi/T$ is oscillating. The parameters used in the calculations are: $\alpha = 0.99$; $f_r = 0.99$; $f_c = 0.98$; $\lambda_0 = 2\pi/k_0 = 1.5\,\mu$m; $\xi = 2.5 \times 10^{-8}$; $L_{FUT} = 20\,$cm. Vertical line shows the set point wavelength. Inset: (left) diagram of the all-fiber ring resonator and transmittance vs. wavelength in static conditions; (right) transmittance vs. time at the set point wavelength when the acoustic wave is oscillating.

zero crossing of the sinc function shifts to lower frequencies and ϕ_0^b is modulated strongly and dampens rapidly with increasing frequency. Such a response can be a serious limiting factor when a fiber length of several tens of cm or above is required.

Let us now consider an optical fiber ring resonator having a loop of length L with the interaction fiber section of length L_{FUT} ($L_{FUT} < L$) included in the loop. The phase delay accumulated by the probe beam propagating in the loop when an acoustic mode of frequency Ω is oscillating, can be expressed as,

$$\phi(t) \equiv \phi_{DC} + \phi_{AC}(t) \tag{8}$$

where ϕ_{DC} is the phase delay in absence of acoustic modulation, which is due to the propagation in the ring and coupler. The steady-state transmittance of a ring resonator in which light undergoes a time-dependent phase delay $\phi(t)$ is given by [25],

$$T(t) = |f_c|^2 \left| \alpha - \frac{\beta^2}{\alpha} \sum_{m=1}^{\infty} (\alpha \cdot f_c \cdot f_r)^m \cdot e^{j \sum_{p=1}^{m} \phi(t - p \cdot \tau)} \right|^2 \tag{9}$$

where α, β, and f_c are the direct-, the cross-coupling, and the transmission coefficient, respectively, of the fiber coupler, f_r is the transmission of the fiber ring, and τ is the ring round-trip time. Fig. 2 shows a calculation of the transmittance as a function of optical wavelength around a notch, at different time instants when an acoustic wave of frequency Ω oscillates. The notch swings with time periodically, which causes an oscillation of the transmittance at any given wavelength. In the case of constant phase delay, (9) reduces to the transmittance of the static ring resonator, showing a series of nearly equidistant notches as optical wavelength is scanned, as shown in the inset of Fig. 2.

When the amplitud of $\phi_{AC}(t)$ is small, as it happens when it is caused by an FSBS stimulated acoustic mode, the steady-state transmittance of the ring at a wavelength matching the slope of

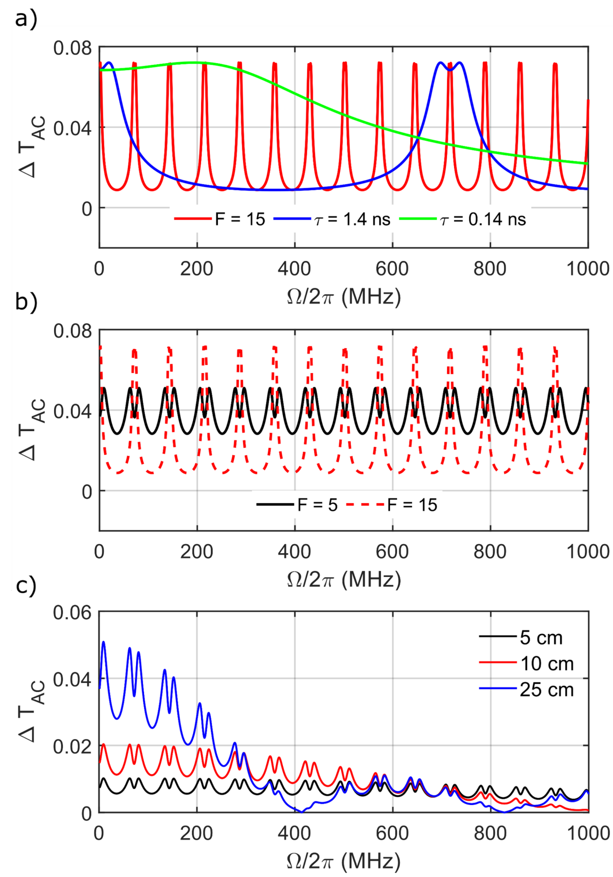

Fig. 3. (a) Oscillation amplitude of the transmittance, ΔT_{AC}, as a function of frequency when acoustic wave and probe beam co-propagate. Calculations for three ring resonators with equal finesse ($F = 15$) and different round-trip time, τ, are shown. (b) ΔT_{AC} for two ring resonators with equal roundtrip $\tau = 14$ ns and different finesse, F. In both, $L_{FUT} = 25$ cm. (c) ΔT_{AC} as a function of frequency when acoustic wave and probe beam counter-propagate. Calculations for three L_{FUT} are shown ($F = 5$ and $\tau = 14$ ns). In all calculations $\xi = 2.5 \cdot 10^{-8}$. The values of α, f_c and f_r were chosen so that the notch depth of the static ring was ~99 %. The probe wavelength was selected to match the linear slope of a transmittance notch as indicated in Fig. 2.

a notch, can be approximatted, to a first order, by

$$T(t) \approx T_{DC} + \Delta T_{AC} \cdot \cos(\Omega \cdot t) \tag{10}$$

where T_{DC} is a constant level that depends on ϕ_{DC}, and ΔT_{AC} describes the oscilation amplitude of the transmittance. ΔT_{AC} depends on the amplitude of ϕ_{AC}, but also on Ω and τ. Fig. 3 shows ΔT_{AC} as a function of Ω for a given effective index modulation amplitude ξ. In the case of co-propagation configuration, ΔT_{AC} shows a periodic oscillating response with Ω (see Fig. 3(a)). This behavior can be understood by considering the multiple beam nature of such an interferometer [25]. The periodicity in frequency depends on the round-trip time, specifically, it is equal to τ^{-1}. The amplitude range of ΔT_{AC} depends on the finesse (F), the higher the finesse, the greater the difference between the maximum and minimum of ΔT_{AC}. For the two examples shown in Fig. 3(b), whose finesse are 5 and 15, the difference between maximum and minimum of ΔT_{AC} are 0.051 and 0.018, respectively. It is worth to note that the frequency response shown for a very short ring resonator is consistent

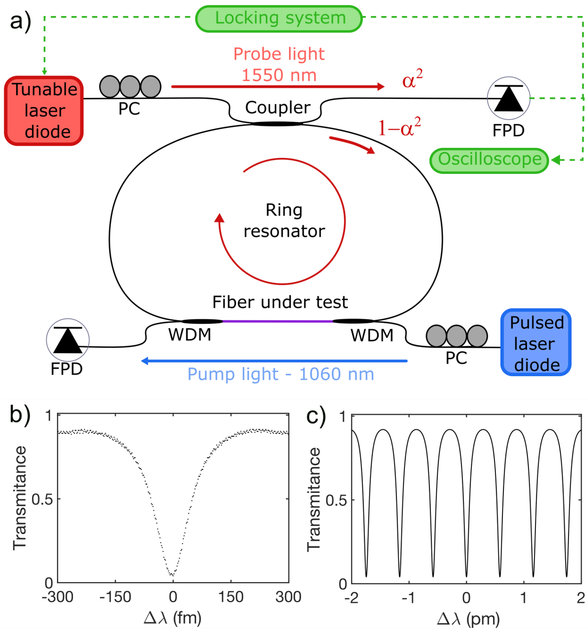

Fig. 4. (a) Experimental arrangement; (b) and (c) show the wavelength transmission response of ring A with no pump signal.

with the response reported for an optical microresonator system supporting WGM resonances [24].

The frequency response in the counter-propagation configuration is more complex, especially for long L_{FUT}, as the amplitude of ϕ_{AC} depends in this case on Ω. Fig. 3(c) shows the frequency response of ΔT_{AC} for three rings of similar characteristics ($F = 5$, $\tau = 14$ ns) but different L_{FUT}. In essence, the frequency response in the counter-propagation configuration is that of the co-propagation configuration but modulated by the frequency response of ϕ_0^b.

In summary, the frequency response of the ring resonator introduces an additional contribution that will shape the amplitude of the probed acoustic modes. Through the design of the ring resonator, this contribution can be tailored, although the sensitivity will change accordingly.

III. Experimental Methods

Fig. 4 shows the experimental arrangement. Two all-fiber ring resonator interferometers were assembled with different directional couplers and loop lengths. Both, the couplers and the loop were made of Corning SMF-28e fiber. Two optical fiber wavelength division multiplexers (WDMs) were inserted into the loop to deliver the optical pump beam to the fiber under test (FUT) and to extract it from the ring, respectively. The FUT consisted of a short section of SMF-28e from which the polymer coating was removed. A directional coupler with a 50:50 coupling ratio was used for ring A, and the total loop length was 2.89 m. Ring B was constructed using a 90:10 directional coupler and the loop length was 2.03 m. A fiber polarization controller (PC) was used to adjust the polarization state of the probe beam in order to optimize the ring transmission notches. The transmission response of one of the rings, without acoustic oscillation (i.e., constant phase delay) is shown in Fig. 4(b) and (c). Table I gives the optical parameters of the static rings' response.

TABLE I
Optical Parameters of All-Fiber Rings

	FSR (fm)	3dB-BW (fm)	Q factor	Finesse	τ (ns)
Ring A	574	104	1.5×10^7	5.5	13.9
Ring B	819	50	3.1×10^7	16.3	9.8

The pump laser used to stimulate the oscillation of the acoustic modes in the FUT was a microchip Q-switch laser that emitted linearly polarized optical pulses of 700 ps duration at 20 kHz repetition rate, with 150 mW average power at 1064 nm wavelength. A set of waveplates was used to control the polarization of the pump.

The oscillation of the acoustic modes in the FUT was optically probed by a single-frequency, tunable diode laser (Koheras BASIK, 100 Hz linewidth) that was fine-tuned to a given set point, typically to the wavelength at which the transmission of a notch is 50% and the slope is maximum. The modulation of the notch that results from the acoustic oscillation leads to the intensity modulation of the probe signal, that was detected and recorded using a fast photodetector (FPD) and an oscilloscope. The spectral components of the probe signal were analyzed with an RF spectrum analyzer. An active locking technique based on an electronic feedback control system was applied to lock the probe signal to the set point and to prevent the effects of low-frequency drift caused by variant environmental conditions. The feedback stabilization method used is based on a power-locking technique and ensures long-term operation. In this method, the deviation of the transmitted power from a set point value is used as a feedback parameter to electronically adjust the probe laser wavelength. A detailed description and demonstration can be found in [26].

To lock the probe laser to a resonance of a given ring, we proceeded as follows: first, a transmission notch was found by scanning the wavelength of the probe laser. As the ring's response is periodic in wavelength with an FSR in the order of a few pm, a short tuning range is required. In our setup, it was done using the built-in fine-tuning facility of the probe laser. Then, the probe laser was tuned to the desired set point. The electrical signal from the photodiode was low-pass filtered and the integral of the error signal -i.e., the difference with respect the set point- is used as the feedback signal. Finally, the reference voltage of the drift compensator electronic circuit was adjusted to match the voltage corresponding to the desired set point.

IV. Results and Discussion

Fig. 5 shows an example of the temporal trace recorded in the oscilloscope after a pump pulse was propagated along the FUT. The probe intensity shows a series of oscillations whose amplitude decays with time. Such oscillations are caused by the stimulation of an acoustic wave packet by the pump pulse. During the first few ns, evidences of cross-phase modulation

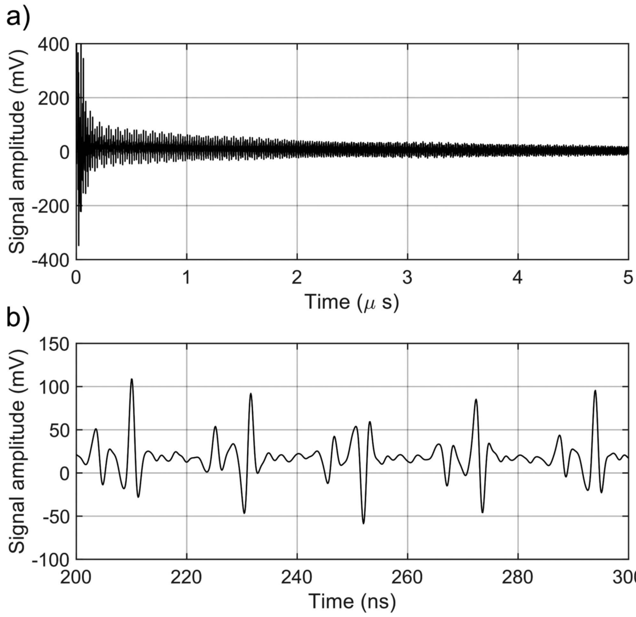

Fig. 5. (a) A temporal trace of the probe signal recorded in the oscilloscope for ring A after a pump pulse propagates along the FUT. (b) A detail of the temporal trace shown in (a). Average pump power: 60 mW; $L_{FUT} = 15\,\text{cm}$.

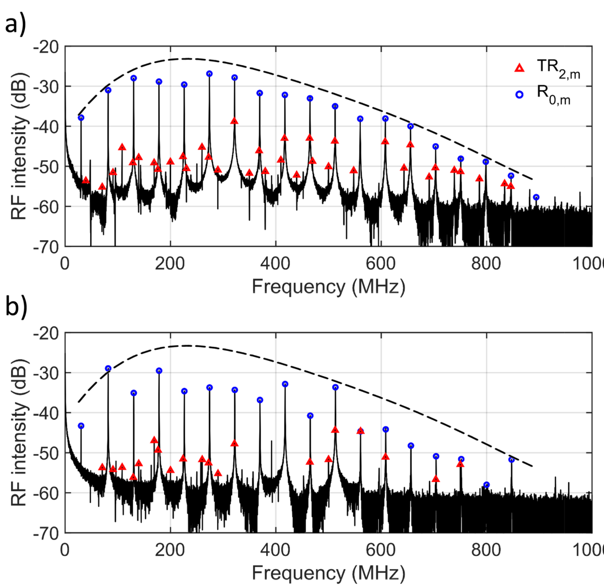

Fig. 6. (a) Measured power spectral density of the probe modulation due to acoustic waves with (a) ring A and (b) ring B. Average pump power: 60 mW; $L_{FUT} = 15\,\text{cm}$. Dashed line shows the expected amplitude profile of radial modes assuming a flat response of ΔT_{AC}.

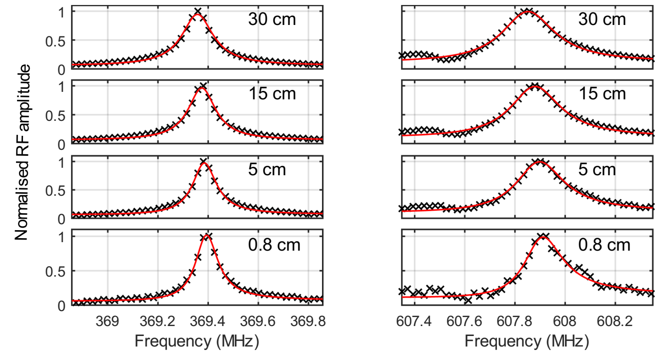

Fig. 7. Normalized RF spectrum (scatter) of resonances $R_{0,5}$ (left) and $R_{0,13}$ (right) for different L_{FUT}, and best-fit to the Breit–Wigner–Fano line-shape (solid line).

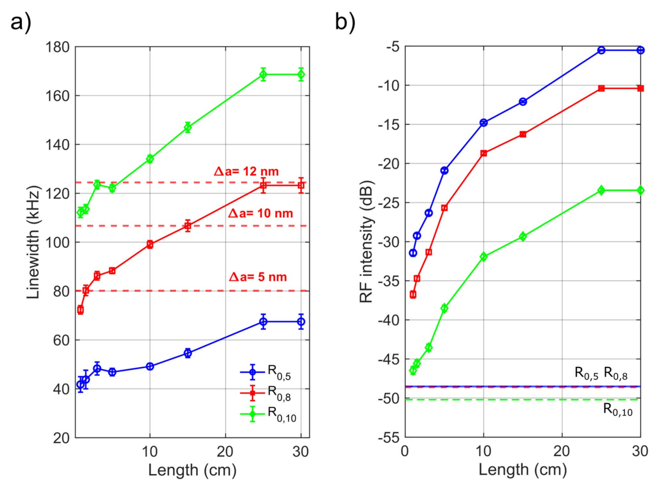

Fig. 8. (a) Linewidth of several resonances as a function of L_{FUT}. Horizontal dashed line shows the theoretical linewidth assuming a fiber radius variation Δa. (b) RF intensity of several resonances as a function of L_{FUT}. Horizontal dashed line shows the noise background measured with $L_{FUT} = 0$ cm. All measurements were performed with ring A and average pump power of 60 mW.

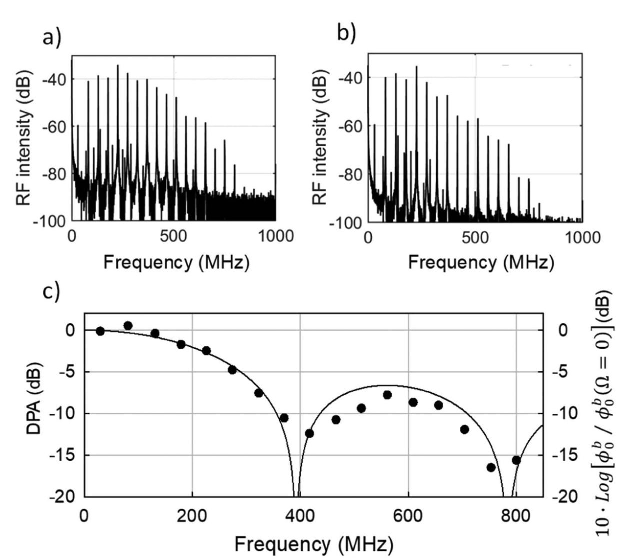

Fig. 9. RF spectrum of the probe signal recorded in (a) co-propagation and (b) counter-propagation configurations at the same pump power. (c) Peaks' amplitude difference (DPA) between both RF spectra (scatter) and normalized ϕ_0^b (solid line) for $L_{FUT} = 25\,\text{cm}$.

(XPM) between the pump and the probe were noticed, as it typically happens when pump and probe signals propagate through the same waveguide.

Fig. 6 shows the power spectral density of two probe signals from ring A and ring B, respectively. To avoid contribution of XPM-induced modulation in the power spectral density, the first few ns of the temporal trace were disregarded before being analyzed by fast Fourier transform (FFT) to obtain the FSBS

TABLE II
COMPARATIVE OF DIFFERENT FSBS PROBING METHODS FOR R0,M ACOUSTIC MODES IN OPTICAL FIBERS

Ref.	Method	Pump power	FUT length	Experimental complexity	Pump scheme
[5]	Sagnac interferometer	~ W[#]	30 m	Low	Pulses
[22]	Narrow-band LPG	~ kW[#]	11 cm	Medium	Pulses
[23]	FBG in multicore fiber	~ W[*]	8 mm	Medium-to-high	AM-modulated for resonant excitation of a single acoustic mode. Synchronous detection
[21]	Sideband Brillouin amplification	~ W[*]	3 mm	High	AM-modulated for resonant excitation of a single acoustic mode
[24]	WGMs	~ kW[#]	< 1 mm	Medium-to-High	Pulses
This work	All-fiber ring resonator	~ kW[#]	4 mm	Medium	Pulses

* Continuous wave; # Pulsed (peak power)

spectrum. It is worth to note that the noise level is slightly affected by the time window used to calculate the FFT. Each peak of the spectrum is caused by the oscillation of an acoustic mode. The peaks with larger amplitude correspond to radial acoustic modes. In this example, up to the $R_{0,19}$ mode whose resonance frequency is 900 MHz was detected unambigously. Although no special care was taken to adjust the pump polarization, a number of torsional-radial modes are shown in both cases. We can observe a certain fluctuation of the peak amplitude in the sequence of radial resonances. The origin of such fluctuation is the frequency response of the ring transmittance (see Fig. 3(a)). The dashed line in Fig. 6(a) and (b) shows the relative amplitude profile calculated under the assumption of a constant ΔT_{AC}, independent of frequency. It can be seen that the deviation of the amplitude of the experimental peaks is more pronounced in the spectrum of Fig. 6(b) corresponding to ring B, which has a higher finesse. This observation agrees with the theoretical model in Section II, where it is shown that the range of variation with frequency of ΔT_{AC} is significantly larger for the ring with higher finenesse (see Fig. 3(b)).

We studied the performance of the probing method as a function of L_{FUT}, focusing on short fiber sections. We aimed to investigate the shortest FUT length that can be probed with this method, keeping in mind applications where fiber length may be a limitation. Also, we studied experimentally the dependence of the linewidth of FSBS-excited acoustic modes on fiber length. Measurements with FUT length varying from few tens of cm to few mm were performed at different pump powers. Care was taken to keep the pump polarization unchanged along the series of measurements. Fig. 7 shows the normalized RF spectrum around acoustic modes $R_{0,5}$ and $R_{0,13}$, for different FUT lengths, at the same pump power. The linewidth and the peak intensity of the resonances in the RF spectrum were obtained from fitting the spectrum of each resonance to a Breit-Wigner-Fano function to account for the asymmetric shape caused by the Kerr effect [27].

Fig. 8 sumarizes the results. It shows the amplitude of peaks in the RF spectrum and the linewitdh of various resonances as a function of FUT length. This series of measurements was performed with a fixed pump power. A significant reduction of linewidth was observed for all resonances as L_{FUT} was decreased. For example, linewidth of $R_{0,8}$ acoustic mode was 124 kHz for $L_{FUT} = 30\,\text{cm}$ and 72 kHZ for $L_{FUT} = 8\,\text{mm}$. We understand that such a evolution is due to the contribution to linewidth broadening of fiber inhomogeneities, which is larger as the fiber length increases. The dashed lines in Fig. 8(a) show the linewidth calculated theoretically for the $R_{0,8}$ acoustic mode in a fiber with a diameter fluctuation of 5 nm, 10 nm and 12 nm, respectively. Contributions to linewidth from glass viscosity [28] and from acoustic impedance mismatch between glass and air [5] were included in the calculation. The comparison between the experimental and theoretical linewidth supports our hypothesis. The theoretical linewidth obtained with the smaller fiber radius fluctuation better describes the experimental linewidth in short fiber lengths, whereas the proper description of linewidth in longer fibers requires increasing the fiber diameter fluctuation range in the theoretical modelling. It is worth to mention that we did not observed changes in linewidth with pump power.

The RF peak amplitude of the resonances decreases with decreasing FUT length, as expected. Dashed lines in Fig. 8(b) indicate the signal background for each resonance which we assumed to be the signal level with $L_{FUT} = 0\,\text{cm}$. For a few cm of fiber, the peak amplitude for most resonances is a few tens of dB above the background level. For the shortest fiber length analyzed in the experiment, 4 mm, a series of peaks corresponding to resonances from $R_{0,2}$ to $R_{0,15}$ could be detected, with amplitudes ranging from 2 to 10 dB above the noise level. Note that these figures are specific to the pump power level and the characteristics of the fiber used in the experiment. In this sense, there are different options to improve the FSBS gain of the resonances, such as the use of nonlinear optical fibers [10] and/or thin-diameter fibers [29].

Finally, we experimentally investigated the impact on the probing of the acoustic modes when they were stimulated with a counter-propagating pump beam. In Fig. 9, the RF spectrum recorded in co-propagation and counter-propagation configurations are compared for $L_{FUT} = 25\,\text{cm}$. Counter-propagation of the pump and probe beams was realized by delivering the pump through the WDM used to extract the pump from the ring in the co-propagation configuration shown in Fig. 4(a). The ratio between the peak amplitude of radial modes in the two configurations is shown in Fig. 9(c). This result shows a very good agreement with the theoretical findings and it faithfully reproduces the dependence with frequency Ω of the amplitude of ϕ_{AC} for the counter-propagating configuration, as depicted in Fig. 1.

A summary of the performance of the present method and other reported results based on different techniques for FSBS excitation and detection of radial acoustic modes is given in Table II. The comparison of performance of the different methods, in terms of minimum fiber length and pump power required, is complex as it also depends on the pump scheme used for the excitation of the acoustic modes. Works based on the resonant stimulation of a single acoustic mode using an amplitude-modulated pump beam [21], [23] report successful $R_{0,m}$ probing with fiber length < 1 cm and pump power level in the order of $\sim$W. When multiple acoustic modes are stimulated by optical pulses, it becomes necessary either the use of a fiber length on the order of tens of meters [5], or a higher level of pump power [22], [24], similar to that used in the present work, if probing is addressed with sub-cm fiber length. It should be noted that the probing method presented in this paper can also be implemented in combination with resonant stimulation of acoustic modes.

V. Conclusion

A versatile, highly efficient approach for the interrogation of FSBS-stimulated mechanical vibrations in optical fibers has been demonstrated. Radial acoustic modes stimulated with low average pump power (few kW peak power) were successfully probed in sub-cm fiber length. By this technique, we performed a detailed investigation of the linewidth broadening of the spectral resonances with fiber the length. This study highlights the impact of fiber inhomogeneities. In the case of the fiber used in the experiment, we observed a reduction in linewidth of approximately 40% when comparing the values measured with 30 cm and with 1 cm of fiber.

The method might be particularly suitable for probing FSBS in other photonic waveguides as for example microstructured optical fibers in which recording of FBGs/LPGs is not straightforward, the availability of sufficiently uniform fiber sections required for a Sagnac interferometer may be limited, and the use of WGMs does not work as the acoustic oscillation is strongly restricted to the core region.

References

[1] Y. London, H. H. Diamandi, and A. Zadok, “Electro-opto-mechanical radio-frequency oscillator driven by guided acoustic waves in standard single-mode fiber,” *Appl. Phys. Lett.*, vol. 2, no. 4, Mar. 2017, Art. no. 041303.

[2] L. A. Sánchez, A. Díez, J. L. Cruz, and M. V. Andrés, “High accuracy measurement of Poisson’s ratio of optical fibers and its temperature dependence using forward-stimulated Brillouin scattering,” *Opt. Exp.*, vol. 30, no. 1, pp. 42–52, Jan. 2022.

[3] G. Bashan, H. H. Diamandi, E. Zehavi, K. Sharma, Y. London, and A. Zadok, “A forward Brillouin fibre laser,” *Nature Commun.*, vol. 13, no.no. 1, Jun. 2022, Art. no. 3554.

[4] Y. Liu et al., “Narrow linewidth all-optical optomechanically microwave oscillator based on forward stimulated Brillouin scattering,” *J. Lightw. Technol.*, vol. 41, no. 16, pp. 5303–5309, Aug. 2023.

[5] Y. Antman et al., “Optomechanical sensing of liquids outside standard fibers using forward stimulated Brillouin scattering,” *Optica*, vol. 3, no. 5, pp. 510–516, May 2016.

[6] Z. Zhang, Y. Lu, J. Peng, and Z. Ji, “Simultaneous measurement of temperature and acoustic impedance based on forward Brillouin scattering in LEAF,” *Opt. Lett.*, vol. 46, no. 7, pp. 1776–1779, Apr. 2021.

[7] Y. Xu, X. Zhao, Y. Li, Z. Qin, Y. Pang, and Z. Liu, “Simultaneous measurement of relative humidity and temperature based on forward Brillouin scattering in polyimide-overlaid fiber,” *Sens. Actuators, B*, vol. 348, Dec. 2021, Art. no. 130702.

[8] L. A. Sánchez, A. Díez, J. L. Cruz, and M. V. Andrés, “Strain and temperature measurement discrimination with forward Brillouin scattering in optical fibers,” *Opt. Exp.*, vol. 30, no. 9, pp. 14384–14392, Apr. 2022.

[9] K. Shemer et al., “Optical fiber point sensors based on forward Brillouin scattering,” *Opt. Exp.*, vol. 30, no. 22, pp. 39321–39328, Oct. 2022.

[10] G. Yang et al., “Simultaneous sensing of temperature and strain with enhanced performance using forward Brillouin scattering in highly nonlinear fiber,” *Opt. Lett.*, vol. 48, no. 13, pp. 3611–3614, Jun. 2023.

[11] X. Li, Y. Lu, and Z. Zhang, “Simultaneous measurement of temperature and pressure based on forward Brillouin scattering in double-coated optical fiber,” *J. Lightw. Technol.*, vol. 41, no. 15, pp. 5130–5137, Aug. 2023.

[12] L. A. Sánchez, A. Díez, J. L. Cruz, and M. V. Andrés, “Recent advances in forward Brillouin scattering: Sensor applications,” *Sensors*, vol. 23, no. 1, Jan. 2023, Art. no. 318.

[13] A. Zadok, E. Zehavi, and A. Bernstein, “Opto-mechanical fiber sensing with optical and acoustic cladding modes,” *APL Photon.*, vol. 8, no. 7, Jul. 2023, Art. no. 071101.

[14] R. M. Shelby, M. D. Levenson, and P. W. Bayer, “Guided acoustic-wave Brillouin scattering,” *Phys. Rev. B*, vol. 31, no. 8, pp. 5244–5251, Apr. 1985.

[15] C. Álvarez-Ocampo, M. Delgado-Pinar, A. Díez, J. L. Cruz, and M. V. Andrés, “Experimental study towards the development of highly sensitive opto-mechanical sensors based on FSBS in telecom optical fibers,” *Opt. Exp.*, vol. 32, no. 23, pp. 41984–41992, Nov. 2024.

[16] A. Zadok, H. H. Diamandi, Y. London, and G. Bashan, *Forward Brillouin Scattering in Standard Optical Fibers: Single-Mode, Polarization-Maintaining, and Multi-Core, (Springer Series in Optical Sciences)*. New York, NY, USA: Springer, 2022, vol. 240.

[17] M. C. Estevez, M. Alvarez, and L. M. Lechuga, “Integrated optical devices for lab-on-a-chip biosensing applications,” *Laser Photon. Rev.*, vol. 6, no. 4, pp. 463–487, Jul. 2012.

[18] D. M. Chow and L. Thévenaz, “Forward Brillouin scattering acoustic impedance sensor using thin polyimide-coated fiber,” *Opt. Lett.*, vol. 43, no. 21, pp. 5467–5470, Nov. 2018.

[19] H. H. Diamandi, Y. London, G. Bashan, and A. Zadok, “Distributed optomechanical analysis of liquids outside standard fibers coated with polyimide,” *Appl. Phys. Lett. –Photon.*, vol. 4, no. 1, Jan. 2019, Art. no. 016105.

[20] W. Zhang, Y. Lu, and C. He, “Simultaneous measurement of temperature, refractive index, and axial strain based on forward Brillouin scattering in polyimide-coated SMF,” *IEEE Sensors J.*, vol. 23, no. 22, pp. 27361–27368, Nov. 2023.

[21] T. Li et al., “3-mm recognition capability of forward stimulated Brillouin scattering measurement by Brillouin selective sideband amplification,” *J. Lightw. Technol.*, vol. 42, no. 2, pp. 898–906, Jan. 2024.

[22] L. A. Sánchez, A. Díez, J. L. Cruz, and M. V. Andrés, “Efficient interrogation method of forward Brillouin scattering in optical fibers using a narrow bandwidth long-period grating,” *Opt. Lett.*, vol. 45, no. 19, pp. 5331–5334, Oct. 2020.

[23] H. H. Diamandi et al., “Opto-mechanical interactions in multi-core optical fibers and their applications,” *IEEE J. Sel. Top. Quantum Electron.*, vol. 26, no. 4, Jul./Aug. 2020, Art. no. 2600113.

[24] L. A. Sánchez, M. Delgado-Pinar, A. Díez, and M. V. Andrés, “Forward Brillouin scattering spectroscopy in optical fibers with whispering-gallery modes,” *Adv. Opt. Mater.*, vol. 12, no. 4, Feb. 2024, Art. no. 2301629.

[25] Z. K. Ioannidis, P. M. Radmore, and I. P. Giles, “Dynamic response of an all-fiber ring resonator,” *Opt. Lett.*, vol. 13, no. 5, pp. 422–424, May 1988.

[26] T. Carmon, T. J. Kippenberg, L. Yang, H. Rokhsari, S. Spillane, and K. J. Vahala, “Feedback control of ultra-high-Q microcavities: Application to micro-raman lasers and micro-parametric oscillators,” *Opt. Exp.*, vol. 13, no. 9, pp. 3558–3566, May 2005.

[27] J. Wang, Y. Zhu, R. Zhang, and D. J. Gauthier, “FSBS resonances observed in a standard highly nonlinear fiber,” *Opt. Exp.*, vol. 19, no. 6, pp. 5339–5349, Mar. 2011.

[28] D. Royer, D. Morgan, and E. Dieulesaint, *Elastic Waves in Solids I:FRee and Guided Propagation (Advanced Texts in Physics)*. New York, NY, USA: Springer, 1999.

[29] L. Zhang et al., “Towards high-sensitivity and high-accuracy forward Brillouin scattering-based optomechanical temperature sensing in thin-diameter fibers,” *Opt. Exp.*, vol. 32, no. 1, pp. 586–598, Jan. 2024.